Precision Engineering 36 (2012) 339–348

Contents lists available at SciVerse ScienceDirect

Precision Engineering

journal homepage: www.elsevier.com/locate/precision

Technical note

Feed-system autotuning of a CNC machining center: Rapid system identification and fine gain tuning based on optimal search

Dohyun Kim*, Do Hyeon Son[1], Doyoung Jeon

Department of Mechanical Engineering, Sogang University, 1 Sinsu-dong, Mapo-gu, Seoul 121-742, Republic of Korea

ARTICLE INFO

Article history:
Received 4 January 2011
Received in revised form
14 September 2011
Accepted 29 September 2011
Available online 6 October 2011

Keywords:
Autotuning
System identification
Multiharmonic perturbation signal
PID control
Digital control
Optimal search
Pole-placement method
CNC machining center
Feed system

ABSTRACT

We report an autotuning technique for feed systems of a CNC machine tool using a least-square parametric system identification, a frequency-domain design method, and a fine-tuning method based on an optimal search algorithm. The feed system of a movable-column-type vertical machining center has a large moving mass because spindle and *z*-axis servo systems are housed in the column. Therefore, perturbation signal is carefully designed. Using a reasonably "smooth" multiharmonic signal, system identification is completed rapidly (8 s) without causing excessive vibration or violating travel limits. Accurate information on the plant dynamics is obtained up to 30 Hz. Feed systems (i.e., *x*, *y*, *z* axis) are modeled as 3rd-order transfer functions in a discrete domain, and compared with the identification results obtained using a Gaussian random sequence and a frequency-domain system-identification method. A proportional (P) controller is designed using numerical search in frequency domain that maximizes the tracking bandwidth and still keeps the system well damped. The frequency response is improved compared to that of a pole-placement method ($\zeta = 0.707$). P controllers of all the three axes that minimize contour error for three-dimensional a 20-mm-diameter circular trajectory are fine-tuned using a fast optimal-search method (440 s). The contour error is significantly improved (average error of 2.25 μm), compared to the results of the pole-placement method (37.89 μm) and the frequency domain design method (12.37 μm) when feed rate is 0.5 m/min. The calculated stability margins of the controller gains are satisfactory.

1. Introduction

The importance of CNC machine tools in modern manufacturing cannot be overstated. Control of a servomechanism of CNC-aided machines is fundamental yet important because it coordinates multiple feed axes to track a three-dimensional tool path accurately to ensure the quality of machined workpieces [1]. As global competition calls for faster production cycles than ever, a high-speed high-precision motion control is still an indispensable aspect of CNC machine-tool design.

Although some high-end modern motion controllers feature advanced control schemes, for example friction compensation and acceleration feedforward, their feedback control scheme is either a P (proportional) or PD (proportional-derivative) control in many cases [2,3]. More sophisticated model-based features such as ZPETC (zero-phase-error-tracking control), CCC (cross-coupled control), disturbance cancellation, MRAC (model-reference adaptive control) are not sufficiently transferred to the industry [4]. The feedforward ZPETC controller was proposed to expand the tracking bandwidth by canceling closed-loop poles, and modifying future references based on an inverse of closed-loop dynamics [5–7]. However, the accuracy of a system model is critical for this approach to be successful [8,7]. Furthermore, the feedforward action can create high-frequency components in the reference, and result in a significant vibration in the servomechanism [2,4] unless smoothing up the reference. A disturbance observer is proposed to make the controller robust to parameter variations [2,6], and enhance tracking capability by compensating friction, especially where a speed of at least one axis approaches zero [6,7]. However, this approach is also based on the premise that the system dynamics and friction are precisely modeled. Thus, inaccurate modeling may degrade overall performance [8]. In industrial practice, a P or PD controller is still used for a typical machine-tool specification because these controllers are easily tuned and highly robust [4]. Therefore, a simple yet practical P controller is chosen in this work.

Regardless of the dominant usage, the design of a PID controller is still done heuristically, or done manually with a provided guideline [9]. Furthermore, fine tuning of the controller takes a long

* Corresponding author. Present address: Bioengineering Department, University of California, Berkeley, 342 Stanley Hall, Berkeley, CA 94720, United States. Tel.: +1 510 647 4353; fax: +1 510 642 5835.
E-mail address: dohyun@berkeley.edu (D. Kim).
[1] Present address: VSI Group, Data & Storage Laboratory, LG Electronics Inc., 221 Yangjae-dong, Seocho-gu, Seoul 137-130, Republic of Korea.

0141-6359/$ – see front matter © 2011 Elsevier Inc. All rights reserved.
doi:10.1016/j.precisioneng.2011.09.007

time, and the controller should be retuned if the plant dynamics changes. Thus, there has been a strong thrust on tuning controller automatically [9–15] since the Ziegler–Nichols method was introduced in 1942 [16]. All autotuning methods are essentially automation of three separate design steps. Firstly, a model structure is defined. Time-domain models include first-order-plus-dead-time models [10], impulse response models [11], higher-order linear transfer functions in a continuous domain [14,13,12], and those in a discrete domain. Frequency-domain models are also used [15,17]. Secondly, the input-to-output characteristics (either parametric or nonparametric) of a system is identified. For this purpose, various perturbation signals such as step responses [13], PRBS (pseudo-random binary sequence) [11], RGS (random Gaussian sequence) [18], relay excitations [10,17], sinusoids [14], variable-frequency sinewaves [15] and sweep sines are applied to the plant, and the resulting output signals are collected. Then, the plant model is estimated based on input and output sequences. Thirdly, a controller is designed. In time domain, the design approaches include heuristic rules and tuning formulae [10], desired closed-loop characteristics [11], fuzzy rules [13], placement of closed-loop poles, and cancellation of these poles [9,12,14]. In a frequency domain, tuning rules (e.g., Ziegler–Nichols) [11], and phase- and amplitude-margins criteria were adapted [15,17]. In practice, all these methods may require some sorts of fine tuning before commissioning [9,11].

Many of the aforementioned autotuning methods [16,10,11,13,17] may not be adequate for a certain class of feed systems. In the "movable-" or "traveling-column-type" vertical machining center, a workpiece is mounted on a fixed table. In this configuration, spindle axis and sometimes *z*-axis servo system are housed in the column, and the extremely large mass travels in multiple axes [19]. Therefore, perturbation signals must be reasonably "smooth" not to severely agitate the heavy column. "Aggressive" signals such as RGS, PRBS, high frequency sine steps or sine sweeps could cause an extreme vibration, ball-screw damage, and motor overload. For the same reason, abrupt signals such as step and relay excitation may not be used. Basic relay methods provide information on system dynamics at a single frequency [20]. Open-loop system identification is sensitive to disturbance [15], and may cause violation of travel limits, which can be especially damaging for the movable-column-type machine tools. Conventional least-square fitting of frequency response using sweep sines or step sines over a wide frequency range takes a long time. A novel contribution of this work is a multiharmonic perturbation signal that completes identification rapidly (~8 s), minimizes vibration, and does not violate travel limits.

Maximizing the closed-loop performance of an individual axis does not necessarily guarantee to meet an important design criterion, contour error [2]. An autotuning method developed for a single axis may not be suitable for the case where multiple axes need to be coordinated to minimize contour error. By matching closed-loop dynamics of two axes (i.e., matching magnitude and phase difference), the contouring error can be improved [21] for two dimensional trajectories. Assuming axis models are very accurate, axis matching can be predicted using numerical methods. Although this idea can be readily generalized to the 3-Cartesian axis case, a direct analytical- or simulation-based design might not always be successful in mitigating the contour error when there is discrepancy between the actual and modeled axis dynamics. As the final step of the autotuning procedure, a fine-tuning method for three feed axes that minimizes experimentally obtained contour error using an optimal search algorithm (i.e., steepest-descent algorithm), is proposed. The proposed search method is much faster (~440 s) than a global search where all possible gain combination is examined, and significantly improves the contour error from the results where frequency response of an individual axis is maximized.

Autotuning procedure in this work is summarized as follows: (1) 3rd-order discrete transfer functions of feed systems are acquired using a least-square parametric closed-loop system-identification method and a multiharmonic perturbation signal (Section 3). (2) A P controller that maximizes tracking performance is designed using a pole-placement technique (i.e., $\zeta = 0.707$) and a numerical search algorithm is used for the maximum closed-loop frequency response (Section 4). (3) Fine tuning of *x*, *y*, and *z* axes is performed automatically using an optimal design approach to minimize contour error to a 3-D circular trajectory (Section 5). The fine-tuning method is evaluated in terms of contour-error improvement, compared with the P controllers designed in Section 4.

2. Experimental apparatus

The plants are *x*-, *y*-, and *z*-axis feed systems of a vertical machining center, ACE-V30 (Daewoo Heavy Industries, Incheon, South Korea). The vertical machining center is a "movable-column" type. A workpiece is mounted on a fixed table. A spindle axis and *z*-axis feed are housed in the column. An incremental rotary encoder (10,000 pulse per revolution, TTL signal) was used in each axis for position measurement (lead-screw pitch: 1 encoder pulse = 1 μm). The autotuning algorithm was implemented using a motion-control DSP system (Model DS1003) equipped with an encoder board (Model DS3001) and a DAQ board (Model DS2201), all of which were made by DSPACE Inc. (Wixom, MI, USA). The sampling rate was 4 ms. The autotuning algorithm was written in C language. A PC-software package, Cockpit and Trace (DSPACE), was used to communicate with the DSP system for monitoring of the autotuning procedure. Numerical simulations were written and run in MATLAB (The MathWorks, Inc., Natick, MA, USA).

3. System identification

A feed-system model is identified by observing correlation between input perturbation signal and resulting output of a plant. The model structure has three requirements: (1) physically meaningful; (2) accurately representing the plant dynamics within a frequency range of interest; (3) relatively simple so that the controller can be designed without too much complexity. The perturbation signal is designed cleverly so that accurate model information can be rapidly identified without upsetting the plant.

3.1. Model transfer function

A linear time-invariant transfer function between feed-drive input $U(s)$ (i.e., velocity command) and angular velocity $\Omega(s)$ can be expressed as a 3rd-order system in Laplace domain [22–24]. An integral term s is multiplied to the denominator when expressing output as rotational angle $\Theta(s)$. The transfer function becomes 4th-order system when the position $Y(s)$ is output as $Y(s) = P_l \Omega(s)/s$, where P_l is the lead-screw pitch. Dynamics of the current-feedback loop in a motor drive can be neglected because of a high bandwidth [8,6,7]. The structural modes of lead-screw-nut-type feed axis, usually observed in high frequencies (>100 Hz [25]), are not modeled because: (1) a closed-loop bandwidth (CLBW) of a typical (i.e., not for high-speed machining) CNC machine is about 25 Hz (Our exhaustive heuristic gain tuning resulted in CLBW less than 20 Hz for all feed axes) [4]; (2) power spectrum of reference trajectory for a typical machine tool mainly consists of low frequency signal because the CNC controller generates a trajectory, of which acceleration is limited [18]. Therefore, the transfer function can be practically expressed as a 2nd-order, or 3rd-order system if

time delay at input of the feed drive is considered. The sampling rate T_s was reasonably selected (4 ms, Nyquist frequency = 125 Hz) because: (1) a low attainable CLBW; (2) limited processing power of the DSP system for complex autotuning algorithm; (3) faster sampling is not always better [26,27,18].

3.2. Modified prediction-error method for system identification

An nth-order transfer function of a feed system in z-domain $G_p(z)$, considering the effect of the zero-order hold (ZOH), is expressed as:

$$\frac{Y(z)}{U(z)} = G_p(z) = \frac{b_1 z^{n-1} + b_2 z^{n-2} + \cdots + b_n}{z^n + a_1 z^{n-1} + \cdots + a_{n-1} z + a_n} \quad . \tag{1}$$

Therefore, an auto-regression-with-extra-input (ARX) model is an adequate model structure:

$$y(k) = -\, a_1 y(k-1) - \cdots - a_n y(k-n) + b_1 u(k-1) + \cdots + b_n u(k-n) + v_o(k) \ , \tag{2}$$

where $v_o(k)$ is disturbance, and k is sample counter. The ARX model (Eq. (2)) can be expressed in a vector form:

$$y(k) = \phi^T(k)\theta_o + v_o(k) \quad , \tag{3}$$

where

$$\phi(k) = [-y(k-1) \ \cdots - y(k-n) \quad u(k-1) \cdots u(k-n)]^T \ , \text{ and}$$
$$\theta_o = [a_1 \ a_2 \ \cdots \ a_n \quad b_1 \ b_2 \cdots \ b_n]^T \ .$$

Here θ_o is the parameter for the actual (nominal) system.

Using the prediction-error method (PEM) with a least-square criterion, parameters of the plant model that minimize the difference between the output of the actual system [28] is:

$$\theta_N^{LS} = \left[\frac{1}{N}\sum_{k=1}^{N} \phi(k)\phi(k)^T\right]^{-1} \left[\frac{1}{N}\sum_{k=1}^{N} \phi(k) y(k)\right] = \mathbf{\Phi}^{-1}\mathbf{Y} \ , \tag{4}$$

where N is the total number of samples. However, θ_N^{LS} and θ_o are not identical due to disturbance $v_o(k)$, nonlinear effects, and noise [29]. Thus, θ_N^{LS} may contain biased parameters, which could render unstable the neutrally stable pole originated from integrating action of a motor controller. Thus, this pole should be fixed at $z = 1$ for the stability. Eq. (1) is modified as:

$$\frac{Y(z)}{U(z)} = \frac{b_1 z^{n-1} + b_2 z^{n-2} + \cdots + b_n}{\left(1 - z^{-1}\right)\left(z^n + a'_1 z^{n-1} + \cdots + a'_{n-2} z^2 + a'_{n-1} z\right)} \ , \tag{5}$$

where $a_1 = (a'_1 - 1)$, $a_2 = (a'_2 - a'_1)$, …, $a_{n-1} = (a'_{n-1} - a'_{n-2})$, and $a_n = -a'_{n-1}$. This transfer function is rewritten for the least-square formulation:

$$\frac{\Delta Y(z)}{U(z)} = \frac{Y(z) - Y(z-1)}{U(z)} = \frac{b_1 z^{n-1} + b_2 z^{n-2} + \cdots + b_n}{z^n + a'_1 z^{n-1} + \cdots + a'_{n-2} z^2 + a'_{n-1} z} \ , \tag{6}$$

and

$$\Delta y(k) = \phi_r^T(k)\theta_{ro} + v_o(k) \ , \tag{7}$$

where

$$\phi_r(k) = [-\Delta y(k-1) \ \cdots \ - \Delta y(k-n+1) \quad u(k-1) \cdots \ u(k-n)]^T \ ,$$
$$\theta_{ro} = [a'_1 \ \cdots \ a'_{n-1} \quad b_1 \cdots b_n]^T \ , \text{ and}$$
$$\Delta y(k) = y(k) - y(k-1).$$

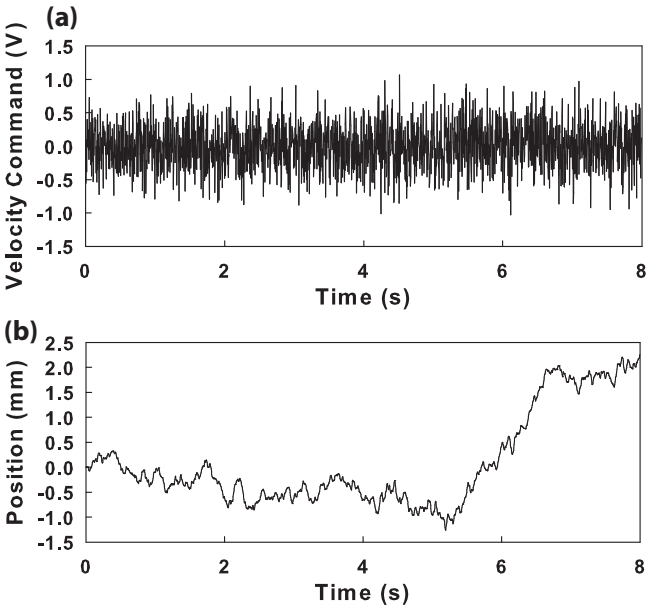

Fig. 1. (a) A Gaussian pseudo-random input sequence and (b) the output of the x-axis feed system.

Least-square estimation of the model parameter

$$\theta_N'^{LS} = [\hat{a}'_1 \ \cdots \ \hat{a}'_{n-1} \quad \hat{b}_1 \cdots \hat{b}_n]^T \ , \tag{8}$$

is again attained using PEM. The original model (Eq. (1)) is recovered from $\theta_N'^{LS}$.

3.3. Multiharmonic perturbation signal

Perturbation signal $u(k)$ is applied to the plant $G_p(z)$ (i.e., feed system) and plant output $y(k)$ is collected for system identification. Here, $u(k)$ is velocity command (unit of V) to the servo drive, and $y(k)$ is position (unit of μm) obtained from encoder reading. A persistent excitation condition must be met for $u(k)$ to ensure the identifiability of a given model [28]. Usually, signals with constant spectra such as PRBS or RGS (Fig. 1a) were considered to be better owing to excellent persistence-excitation orders. However, such "flat-band" random sequences have some drawbacks. The flat-band signal could lead to a bias toward high frequency in an ARX model structure [18]. Also, such aggressive signals are not suitable for a class of CNC machining centers. When the inertia of the column is very large, RGS caused an extreme vibration (Fig. 1b), which could damage the lead screw and overload the servo motor. The conventional swept sine excitation of a wide band was not an exception in this regard.[2] Furthermore, the column drifted and sometimes hit the travel limit because of a long duration (>10 min). Additionally, swept sine excitation is sensitive to nonlinear distortion [29].

Therefore, the input signal should be designed carefully. Firstly, the signal must be "smooth" enough to minimize such excessive vibration. Secondly, the signal must be informative by having a wide range of frequency components [28]. Thirdly, the signal should be symmetric so that a feed axis would not reach the travel limit. Lastly, for rapid system identification, N should be an acceptable number (i.e., duration of the signal should be reasonably short). A multiharmonic signal, the combination of weighted sinusoids of

[2] In an actual instance, graduate students in the lab a floor above called emergency because they thought of having an earthquake.

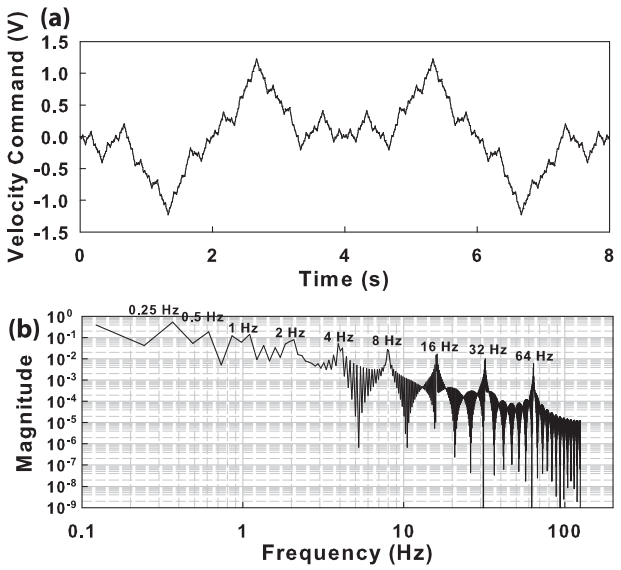

Fig. 2. (a) The multiharmonic input sequence and (b) its discrete Fourier transform (single-sided amplitude spectrum).

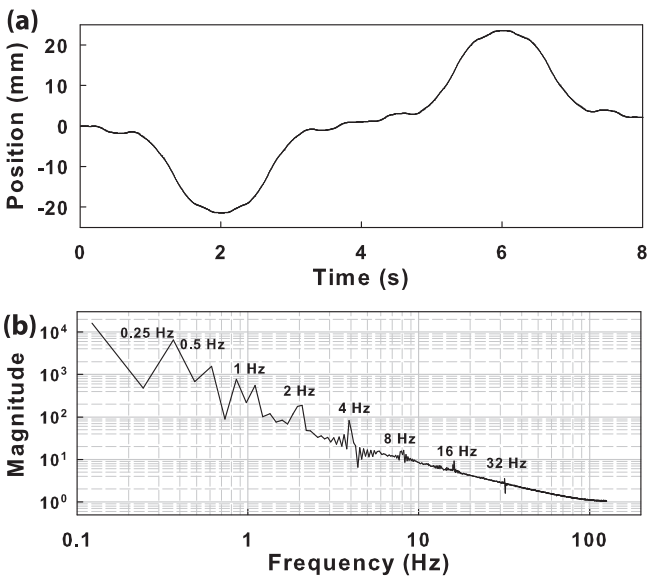

Fig. 3. (a) The output sequence for the *x*-axis feed system to the multiharmonic signal and (b) its discrete Fourier transform (single-sided amplitude spectrum).

various frequencies, is proposed here to meet the aforementioned requirements. The input sequence is defined as:

$$u(k) = \begin{cases} \displaystyle\sum_{i=1}^{n} (-1)^i A^i \sin\left(\frac{2\pi k}{N} 2^i\right) & \text{if} \quad 1 \le k \le N/2, \\ u(N-k+1) & \text{if} \quad (N/2+1) \le k \le N, \end{cases} \tag{9}$$

where the amplitude A is a design parameter. A should be less than 1, so the amplitude is smaller at higher frequencies to minimize the vibration, and $u(k)$ is within the voltage input limit of the servo controller (i.e., ±10 V). On the other hand, if A is too small, signal power is too low to acquire the plant information at higher frequencies. Thus, $A = 1/1.7$ was chosen empirically. As denoted from Eq. (9), the first half of the signal is reversed in the second half. As a result, the perturbation signal is symmetric, forcing the feed axis to return to the origin. In Eq. (9), the 2^i term spreads harmonics logarithmically to cover a wide band with a relatively small n. n should be reasonably large because persistent-excitation order $2n$ should be greater than the number of the parameters to be identified (i.e., $2n$ for the nth-order model) [28]. On the other hand, the highest frequency should be less than the Nyquist frequency (i.e., 125 Hz in this work) to prevent anti-aliasing [30]. Therefore, for $n = 9$ the system parameters were successfully obtained using the PEM. System identification was fast compared to common sweep sine methods; data collection just took 8 s, and parameter calculation was instant. The designed input sequence is shown in Fig. 2a. The discrete Fourier transform (Fig. 2b) shows the logarithmically spread frequency content (i.e., 0.25–64 Hz). It should be noted that the coefficients at low frequency (0.25 and 0.5 Hz) are noisy due to low N.

As seen in Fig. 3a, the open-loop response of the x axis to the perturbation signal does not contain strong high-frequency components unlike random sequences (Fig. 1a). The reduction of high frequency contents is observed in a Fourier transform plot (Fig. 3b). The symmetric output sequence (Fig. 3a) indicates that the axis command returns to the origin.

3.4. Closed-loop system identification

The feed-drive systems are not completely symmetric. The servo-drive input may have non-negligible offset, and frictional and viscous damping can be direction dependent [8,6]. Especially, the z axis is significantly asymmetric due to gravity acting on the heavy column. As a result, the identified parameters θ_N^{LS} could be biased.

The asymmetry and disturbance can be mitigated by using closed-loop system identification. The block diagram (Fig. 4) shows how the perturbation signal is fed to $G_p(z)$, the open-loop transfer function between motor-drive velocity command $u(k)$ and axis position $y(k)$. In this work, the perturbation signal is applied to the loop as position reference $r(k)$. The input–output relationship of the block diagram is expressed as $y(k) = G_c(z)r(k)$, where $G_c(z)$ is the closed-loop transfer function. The gain K_p was set as a small value (= 0.0015). The sequence $r(k)$ was scaled so that the magnitude of the plant input sequence $u_{open}(k)$ is matched with the original perturbation signal (Eq. (9)): $r(k) = u_{open}(k)/K_p$. The closed-loop identification was used for the z axis, as the open-loop identification delivered satisfactory results for the x and y axes.

3.5. Identification results

The 2nd, 3rd, 4th, and 5th-order $G_p(z)$ of the x-, y-, and z-axis feeds are obtained using the PEM and multiharmonic signal. A Bode plot (Fig. 5) shows the system-identification result for 3rd-order model of the x-axis feed (the reason for selecting the 3rd-order model will be given in the next section). As a comparison, the transfer-function estimate obtained using a power spectral method [18] at the 9 frequencies of the multiharmonic perturbation signal is also shown in magnitude plot (Fig. 5a). Except two low-frequency points marked in open circle (perhaps due to small N), the estimate is close to the model, indicating that the identification result is accurate in the frequency domain. A third-order model was obtained using a short RGS signal ($N = 2000$) for the sake of comparison. The

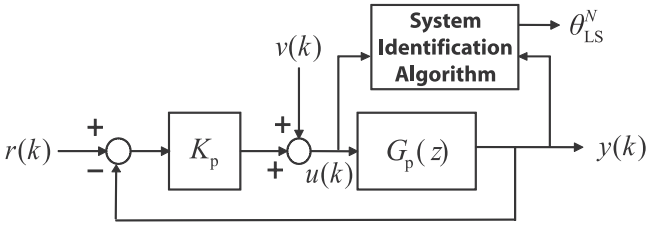

Fig. 4. The block diagram for the closed-loop system identification.

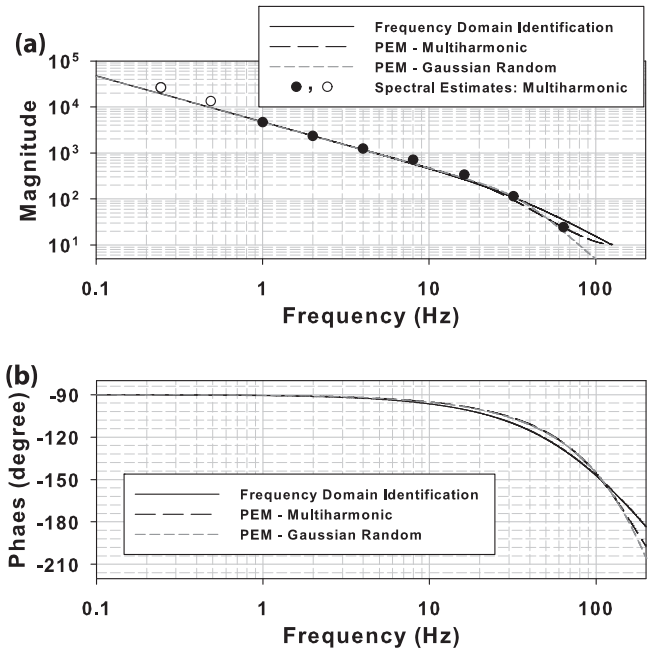

Fig. 5. Comparison of system identification results for the *x*-axis feed in a Bode plot: (1) frequency-domain system identification with a dynamic signal analyzer, (2) prediction error method (PEM) with the multiharmonic signal, (3) PEM with a random Gaussian sequence, and (4) spectral estimate from the multiharmonic input and resulting output sequences.

two models are similar up to 30 Hz, which is higher than the frequency range of interest (~20 Hz). A frequency domain model was also obtained with a dynamic signal analyzer (HP35670A, Agilent, Santa Clara, CA, USA). Due to the aforementioned vibration and travel-limit issues, the maximum frequency was limited to 15 Hz, and the closed-loop identification was performed with a small P gain (0.0005). This model was also very close to the case of the PEM with multiharmonic signal up to 30 Hz. Phase diagram (Fig. 5b) also shows that the model obtained using the PEM and multiharmonic signal is similar to those yielded using the PEM and RGS, and frequency domain modeling, within the frequency range of interest.

The system identification was repeated at least 10 times for each axis, and resulted in stable models everytime. The modified regressor in Eq. (7) guarantees the marginal stability of the system containing integral action in the servo drive. If the servo drive was detuned or the feed system had a mechanical problem, an unstable model could be identified. The autotuning program is designed to display open-loop poles, and alert the user if an unstable pole is detected. Thus, the end user can check the feed axis and identify the system again, by changing the parameters of the excitation input.

3.6. Model selection

The position and velocity outputs of the actual plant and the models of different orders (i.e., 2, 3, 4, and 5th order) are compared for the *y* axis in Fig. 6. A slight offset in position exists when returning to the origin (Fig. 6a and b). Other than that, the models agreed well with the actual plant for all the system orders. Velocity responses in Fig. 6c and d also show good agreement (note that the prediction errors are noisy because velocity is calculated by numerical differentiation, not measured using a tachometer), and do not show the drifts observed in the position outputs (Fig. 6b). The proposed modified discrete models (Eq. (5)) represent the feed-drive systems adequately.

Accuracy of the models of different system orders was compared in terms of average position prediction error. The error is defined as $\left(1/N\right)\sum_{k=1}^{N}\left|y(k)-\hat{y}_m^N(k)\right|$ (m = model order), where $y(k)$ is the position output of the actual plant and $\hat{y}_m^N(k)$ is the output predicted using the models. The difference among the models are insignificant. For example, the model errors were 219.93, 222.22, 224.54, and 226.69 μm for $m = 2$, 3, 4 and 5 respectively for the *y* axis. It is more convenient to design a controller with the models of smaller orders. For example, unstable closed-loop poles were obtained with 5th-order models in a pole-placement controller design step, which will be shown in Section 4.1. Thus, 2nd- and 3rd-order models were chosen. Moreover, as described in Section 3.1, these models are physically meaningful in the frequency range of interest. Table 1 shows the obtained parameters of 2nd- and 3rd-order models for all feed axes. As will be shown later (Section 4.2), the 3rd-order model will be used in the autotuning procedure because it leads to a larger attainable closed-loop bandwidth (CLBW).

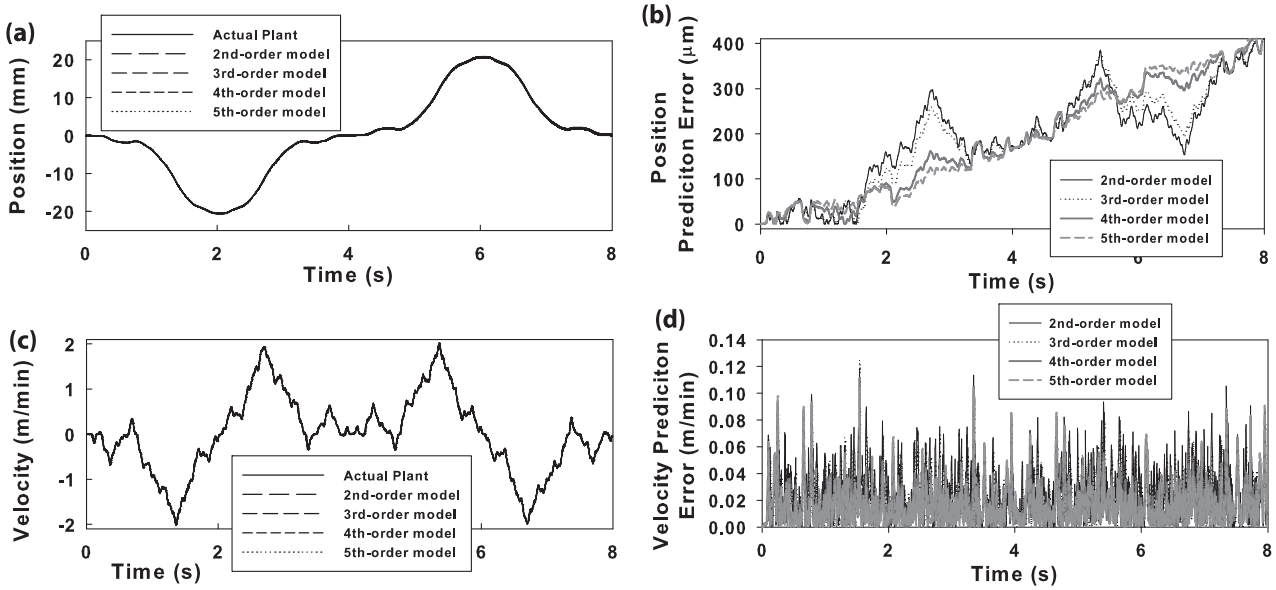

Fig. 6. Comparison of the outputs from the actual plant (*y*-axis feed) and the models of various system orders: (a) position, (b) magnitude of position prediction errors between the actual plant and the model outputs, (c) velocity, and (d) magnitude of velocity prediction error between the actual plant and the model outputs.

Table 1
Model parameters for the *x*-, *y*-, and *z*-feed systems obtained using PEM.

	b_1	b_2	b_3	a_1	a_2	a_3
xaxis						
2nd order	13.60	30.75	–	− 1.624	0.6240	–
3rd order	5.754	39.99	− 18.43	− 2.160	1.553	− 0.3922
yaxis						
2nd order	17.48	22.06	–	− 1.641	0.6410	–
3rd order	10.87	26.40	− 6.971	− 2.032	1.340	− 0.3076
zaxis						
2nd order	10.72	15.53	–	− 1.764	0.7639	–
3rd order	2.442	20.24	− 5.32	− 2.356	1.869	− 0.5129

4. Design of a P controller

Contour error, orthogonal deviation from a desired tool path, is an important metric in the design of motion controllers of a CNC machining center. A design approach is to maximize the CLBW of a feed axis so that the tracking error of each axis is reduced. Expanding the tracking bandwidth of all feed systems leads to the reduction of contour error to curved trajectories [2]. An additional benefit of having a large CLBW is effective rejection of disturbance [31].

4.1. Pole-placement method

Our first design approach is maximizing the CLBW of an individual axis while keeping the closed-loop system well damped. The tracking bandwidth of a 2nd-order system with complex poles is maximized without resonance when the damping ratio is 0.707 [32]. As undamped natural frequency ω_n is the only adjustable variable in such close-loop system, if we find K_p satisfying the 0.707 damping ratio, ω_n is uniquely determined. Therefore, closed-loop poles are distinctively determined.

Poles of a 3rd-order system can be similarly determined. However, a 3rd-order system has an additional pole. The proposed pole-placement method works well for the system where complex poles are dominant second order. The effects of zeros were negligible (i.e., sampling zeros [26], zeros far into the LHP) for feed-drive systems studied in this work. A characteristic equation of the 3rd order system in discrete domain can be written as:

$$(z-r)\left\{z^2 - 2\,e^{-T_s\zeta\omega_n}\cos\left(T_s\omega_n\sqrt{1-\zeta^2}\right)z + e^{-2T_s\zeta\omega_n}\right\} = 0 \quad , \tag{10}$$

where r is the third pole. The above equation should be equal to the characteristic equation of the closed-loop transfer function with a P controller:

$$z^3 + (a_1 + K_p b_1)z^2 + (a_2 + K_p b_2)z + a_3 + K_p b_3 = 0. \tag{11}$$

By equating Eqs. (10) and (11), and arranging them, we have two equations for P gain, $K_{p,1}$ and $K_{p,2}$ as functions of ω_n:

$$K_{p,1}(\omega_n) = \frac{e^{-2T_s\zeta\omega_n} - 2a_3\,e^{T_s\zeta\omega_n}\cos\left(T_s\omega_n\sqrt{1-\zeta^2}\right) - a_2}{b_2 + 2b_3\,e^{T_s\zeta\omega_n}\cos\left(T_s\omega_n\sqrt{1-\zeta^2}\right)} \quad , \text{ and}$$
$$K_{p,2}(\omega_n) = \frac{-2e^{-3T_s\zeta\omega_n}\cos\left(T_s\omega_n\sqrt{1-\zeta^2}\right) - a_1\,e^{-2T_s\zeta\omega_n} + a_3}{b_1\,e^{-2T_s\zeta\omega_n} - b_3} \quad . \tag{12}$$

The above equations can be solved numerically. P gain satisfying $\zeta = 0.707$ can be calculated once ω_n satisfying $K_{p,1}(\omega_n) = K_{p,2}(\omega_n)$ is determined. For the *x* axis, $\omega_n = 123.23$ rad/s, and $K_p = 0.0010826$ at this ω_n. The feedback gains for the *y* and *z* axes were determined in the same way. Table 2 shows the feedback gains and the corresponding CLBWs for all feed axes obtained using the pole placement method as well as other methods which will be described later sections. Predicted stability margins and sensitivity peak for each controller design, which will be elucidated in later sections, are also shown in Table 2.

Table 2
Comparison of P gains and prediction of corresponding stability margins and sensitivity peak obtained using P controller selected in each controller-design step.

Axis	Gains, margins M_s, CLBW	Pole placement	Numerical search	Fine tuning
x	$K_{x,p}$	0.0010826	0.0018931	0.0014747
	GM	6.501	3.718	4.773
	PM (°)	73.39	60.24	67.10
	M_s	1.304	1.603	1.439
	CLBW (Hz)	7.75	18.45	13.21
y	$K_{y,p}$	0.0017102	0.0018733	0.0017732
	GM	5.309	4.847	5.121
	PM (°)	64.33	62.00	63.43
	M_s	1.435	1.484	1.453
	CLBW (Hz)	13.58	15.24	14.24
z	$K_{z,p}$	0.0005230	0.0014326	0.0014145
	GM	9.973	3.641	3.687
	PM (°)	79.43	60.28	60.67
	M_s	1.185	1.609	1.598
	CLBW (Hz)	2.89	13.13	12.96

4.2. Numerical search of P gains in frequency domain

The pole-placement method does not work properly when the assumption of two dominant complex poles fails. The 3rd-order open-loop model has the two complex-conjugate poles, and the one real, marginally stable pole. A root-locus study shows that increasing P gains pulls this real pole toward $z = 0$ and pushes the two complex poles toward the boundary of the unit circle ($|z| = 1$). Thus, setting a P gain using the condition $\zeta = 0.707$ can result the magnitude of the third pole being similar to that of a complex pole. In this case, influence of the third pole cannot be disregarded, and it is difficult to find a P gain that maximizes the CLBW analytically as in the previous section. Thus, a numerical search method is proposed. Firstly, a stable K_p is chosen as an initial condition. A P gain from the pole-placement method can be a good candidate. Secondly, the value of K_p that maximizes the CLBW is numerically found as a function of ω_n using a search algorithm, under the condition:

$$\max_{\omega_n}\left|G_c(e^{j\omega_n T_s}, K_p)\right| \le 1 \quad \left(0 < \omega_n < \pi/T_s\right) \quad , \tag{13}$$

where the CLBW was numerically calculated (i.e., ω_n that satisfies $\left|G_c(\omega_n)\right| = \sqrt{2}/2$). The poles for ω_n are monitored for stability throughout the search process. The search algorithm essentially constructs a bode plot from the model, and thoroughly checks for resonance (i.e., keeps the system well damped) and finds a CLBW. It is found that the bandwidth is improved by increasing K_p as long as the closed-loop poles are stable. Root locus technique was used to confirm this observation.

The P-gains obtained using this method are compared with the gains from the pole-placement method. For the 2nd-order system, the results from the two methods are identical, indicating that the numerical search algorithm works well. For the 3rd-order model (of the *x* axis), however, there is a significant increase in gain (from 0.0010826 to 0.0018931), and an appreciable improvement of frequency response is observed. Thus, the dominant-complex-pole assumption did not work for the *x*-axis. Table 2 also shows the gains for the *y* and *z* axes found in the numerical search method. For the *y*-axis, the results from the two methods are similar, indicating the existence of dominant complex poles. A magnitude plot (Fig. 7) clearly indicates expansion of the CLBW. The 3rd-order system can yield a wider bandwidth than the 2nd-order model can

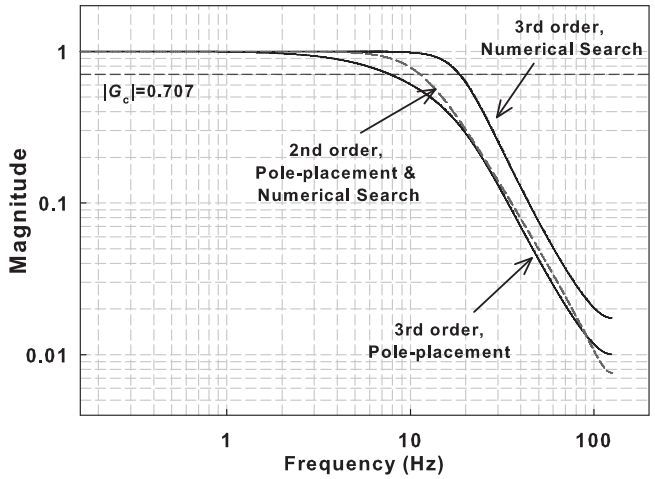

Fig. 7. Closed-loop frequency responses of the 2nd- and 3rd-order models obtained using the pole-placement and numerical search methods (*x* axis).

(i.e., 18.46 Hz vs. 11.28 Hz). Consequently, the 3rd-order model is chosen.

The gain-design methods and model selection proposed here should be valid considering the accuracy of the model (Fig. 5). In addition, model variation should be small because: (1) the machine tool has a fixed payload (i.e., workpiece is mounted on a fixed table); (2) cutting force is delivered thorough a lead-screw-nut system and is at much higher frequency range than the attainable CLBW [33]. Hence the control loop only feels and tries to reject the average value of the cutting forces. Therefore, the gain design method can cope with varying workpiece mass relatively well. Furthermore, as the P gains are selected conservatively (i.e., no resonance), the gain margin is high. A stability margin study will show this point more clearly in Section 5.2.

5. Fine tuning of the P controller

In the previous section, the P gains were selected to maximize the CLBW of each axis. However, contour error would be large if the dynamics of all the axes were not matched. Tracking of a circular trajectory is a common evaluation of contouring performance as the reference signal can be regarded as a linear combination of sinusoid signals. For a two-dimensional circular trajectory, theoretical treatment is available to find optimal closed-loop dynamics [21]. It can be shown that in a 3-Cartesian axis system matching the axis dynamics will result in the tracking errors in the individual axes due to constant velocity motion to be proportional to the commanded velocity components; thereby bringing the tool onto the desired tool path. However, discrepancies between the modeled and true drive dynamics and disturbance forces (like friction or cutting forces) can deteriorate the success of this contour error mitigation strategy. In this case, some manual adjustment of the control gains may be necessary. In this section, the objective is to find optimal P gains that minimize a contour error to a three-dimensional circular trajectory. In practice, this objective can be met by empirical fine tuning of closed-loop dynamics by an operator. Here a rapid, automated fine-tuning method, which can circumvent multi-axis unmatched dynamics, is proposed.

A simple heuristic approach to the aforementioned problem is a global search (i.e., try all possible gains within a given boundary) of the three gains $K_{x,p}$, $K_{y,p}$ and $K_{z,p}$, and choose a gain set that minimizes the contour error. When a three-dimensional circular trajectory is used, the contour error is F:

$$F(K_{x,p}, K_{y,p}, K_{z,p}) = \sum_k \left| r_d - \sqrt{(x(k)-x_0)^2 + (y(k)-y_0)^2 + (z(k)-z_0)^2} \right| \quad , (14)$$

where (x_0, y_0, z_0) is the center and r_d is the radius. The gain of a single axis may be adjusted by a small amount, say 1%, while fixing the other two gains. Then, this procedure is repeated for the remaining axes to find a minimum. However, this sort of a global search would take an impractically long time to finish.

5.1. Optimal-design approach

Optimum design theory [34] is used to find the P gains much faster than the global search. If we express P gains in a vector form $\mathbf{x} = (x_1, x_2, x_3)$ ($x_1 = K_{x,p}$, $x_2 = K_{y,p}$, $x_3 = K_{z,p}$), then the contour error is $F(\mathbf{x})$ (Eq. (14)). Using an optimal design procedure, $\mathbf{x}$ that minimizes $F(\mathbf{x})$ can be found. This specific optimization problem could not be solved using algorithms such as SLP (sequential linear programming) and QP (quadratic programming), because we do not have *a priori* knowledge on the shape of the objective function $F(\mathbf{x})$. As a result, a steepest-descent algorithm (SDA), a gradient descent method, is proposed in this work.

In formulating optimization problem of $F(\mathbf{x})$, the upper bound $\mathbf{x}_u$ are the P gains obtained in Section 4.2, of which the closed-loop response has the maximum CLBW without resonance. By setting the upper bound in this way, the optimal search algorithm is prevented from resulting in excessively underdamped closed-loop response. On the other hand without a proper lower bound, the CLBW can be reduced significantly, causing a poor tracking performance. We propose that the lower bound $\mathbf{x}_l$ is to be specified by a designer: $\mathbf{x}$ that results the lowest allowable CLBW for all axes. The CLBWs obtained in the numerical search method (i.e., upper bound) were 18.46, 15.25, and 13.08 Hz for the *x*, *y*, and *z* axis respectively. Thus the fine tuning will not result in an unstable feed system owing to structural modes typically higher than 100 Hz [25]. The lower bound is chosen to be less than 13.08 Hz for the *z*-axis where the CLBW is the smallest among the axes, but it should not be too small to lose tracking performance significantly. Thus the lower bound was chosen to be 12 Hz in this work.

The initial P gains $\mathbf{x}^{(0)}$ were chosen to be the center point of the solution boundary: $\mathbf{x}^{(0)} = (\mathbf{x}_l + \mathbf{x}_u)/2$. Steepest-descent direction $\mathbf{d}^{(i)}$ that reduces the contour error $F(\mathbf{x})$ fastest is expressed as:

$$\mathbf{d}^{(i)} = -\Delta\mathbf{F}^{(i)}(\mathbf{x}^{(i)}) = \left(-\frac{\partial F}{\partial x_1}\Big|_{x_1=x_1^{(i)}}, -\frac{\partial F}{\partial x_2}\Big|_{x_2=x_2^{(i)}}, -\frac{\partial F}{\partial x_3}\Big|_{x_3=x_3^{(i)}} \right) , \quad (15)$$

where the subscript 1, 2, and 3 denote the *x*, *y*, and *z* axis respectively. The derivatives are calculated numerically using the central-difference approximation since $F(\mathbf{x})$ is not an explicit function. When calculating the central difference, the difference Δx_j ($j = 1, 2, 3$) should be carefully selected. If Δx_j is too small, the amount of the descent becomes excessively large. In this work, Δx_j was chosen 0.1% of the initial P-gains $x_j^{(0)}$. Contour errors were averaged when calculating F to minimize the effects of measurement noise in $y(k)$. The amount of the descent in the direction of $\mathbf{d}^{(i)}$ is determined by an iterative search (i.e., golden-section method [34]). The search completes when the criterion $|\mathbf{d}^{(i)}| < \delta$ is met for a small δ, and then the optimal P gains $\mathbf{x}$ are obtained.

5.2. Fine-tuning result

Fine tuning for the minimum contour error was performed in both numerical simulation and experiment. Fig. 8 shows a test trajectory, a 3-D circle of 20-mm diameter: $(x+r)^2 + (y-z)^2/2 - r_d^2 = 0$, and a tracking result when the P gains are ones

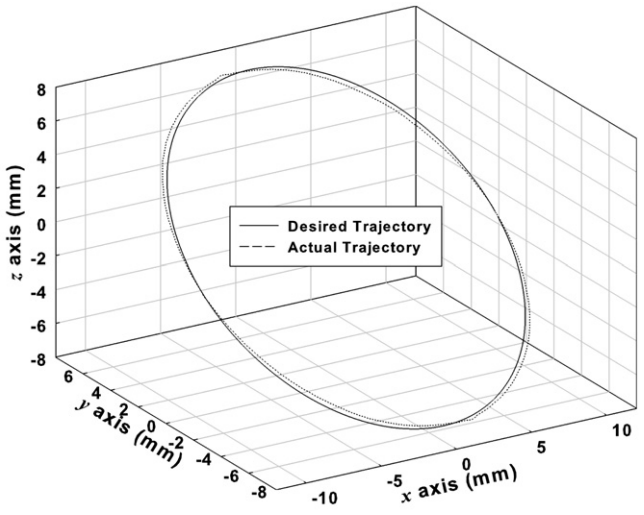

Fig. 8. The 3-dimensional circular test trajectory, and the actual tracking result when P gains were $\mathbf{x} = (0.0010826, 0.0017102, 0.00523)$. The contour error is magnified 10 times.

obtained from the pole-placement method. The upper bound $\mathbf{x}_u$ was (0.0018931, 0.0018733, 0.0014260) (i.e., gains from the numerical search method) and the lower bound $\mathbf{x}_l$ was (0.0013921, 0.0015623, 0.0013213) (i.e., the lowest allowable CLBW = 12 Hz).

Numerical simulation: A simulation code for the SDA was written in MATLAB. The feed rate for all the axes were 0.5 m/min. The initial P gains are: $\mathbf{x}^{(0)} = (0.0016426, 0.0017178, 0.0013736)$, which is the center of the gain boundary. The SDA continues to modify P-gains in the direction of reducing contour error. It only took 5 steps to find the minimum $F(\mathbf{x}) = 0.0038462$, when $\mathbf{x} = (0.0015736, 0.0017515, 0.0014260)$. All predicted CLBWs are similar; the CLBWs were 14.630, 14.015, and 13.068 Hz for the x, y, and z axis respectively.

Experimental result: The fine-tuning method was implemented in the machining center. The identical test trajectory and feed rate were used. The minimum $F(\mathbf{x})$ was found in ~440 s. The final gains are: $\mathbf{x} = (0.0014747, 0.0017732, 0.0014145)$. The gains designed using (1) the pole-placement method ($\zeta = 0.707$), (2) the numerical search method in the frequency domain, and (3) the SDA fine tuning are compared in Table 2.

The gain margin (GM) and phase margin (PM) were also characterized using the open-loop model (Table 1) and P gains obtained in each controller-design method. The GM was from 3 to 10 and the PM was from 60° to 80°. The numerical search method assures that the system, even when the dominant-complex-pole assumption fails, is properly damped by forcing the condition Eq. (13). As the fine tuning algorithm searches feedback gains with the constraint that the upper bound being the value obtained in the numerical search, the PM of system was also satisfactory ($\gg 30°$). The GM and PM values indicate that the control system is adequately

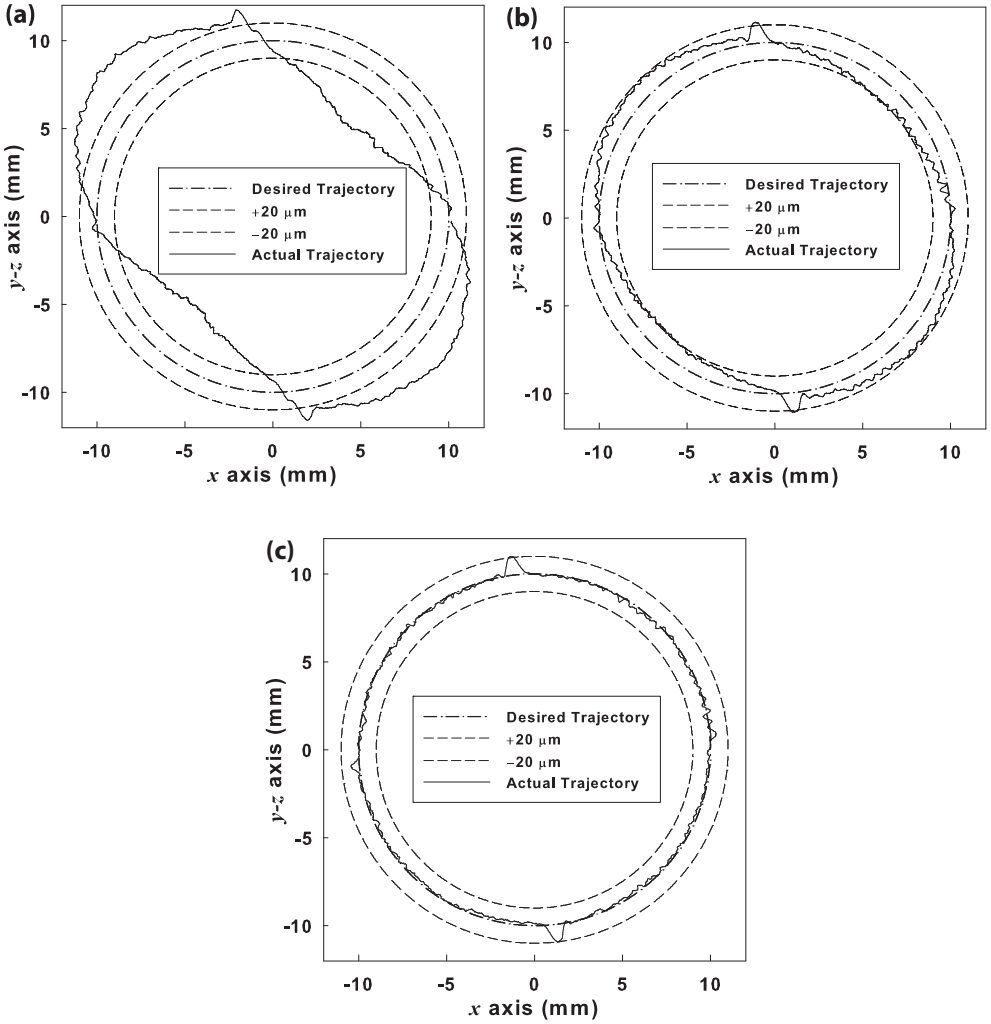

Fig. 9. Contouring results (the contour error magnified 50 times) obtained with (a) the pole-placement method, (b) the numerical search method in frequency domain, and (c) the fine tuning using the steepest-descent algorithm.

Table 3
The average contour errors obtained using P controller obtained in each controller-design step.

	Feed rate	Pole placement	Numerical search	Fine tuning
Average	0.5 m/min	37.89	12.37	2.25
Contour	1 m/min	74.26	24.45	5.15
Error	2 m/min	146.45	48.58	15.50

stabilized in the proposed design methods, and has robustness to model uncertainty, considering the accuracy of the models and the nature of the feed system (i.e., no payload variation, negligible impact from the cutting force). The sensitivity peak M_S was characterized as well, and the value was always less than 1.6. Therefore, it suggests that a disturbance input signal can be well attenuated in the feedback system [35].

The average contour errors acquired for three different feed rates using each of the designed controllers are tabulated in Table 3. The feed rates were 0.5, 1, and 2 m/min. The three-dimensional contouring results (e.g., Fig. 8) are projected onto a two-dimensional plane in Fig. 9 for better illustration when the feed rate is 0.5 m/min. Fig. 9a presents the contour error from the pole-placement design. The CLBW of each feed axis was significantly different (i.e., 7.75, 13.58, and 2.89 Hz for the *x*, *y*, and *z* axis respectively). Therefore, the trajectory was severely elliptical, and the average contour error was the largest (37.89 μm). The numerical search method in frequency domain improved the contour error more than three times (i.e., 12.37 μm, Fig. 9b) as the CLBWs of *x* and *y* axis are much improved. Nonetheless, the elliptical trajectory is still an evidence of "uncoordinated" closed-loop dynamics. The fine-tuning result in Fig. 9c clearly shows that the trajectory is very close to a circle because the feed axes are now well coordinated; the predicted CLBWs are the most similar, comparing with other methods (i.e., 13.21, 14.24, 12.96 Hz for the *x*, *y*, and *z* axis respectively). The contour error is the smallest (2.25 μm), which is more than 16 times improvement over the pole-placement method. This result is encouraging in that the encoder resolution is only 1 μm in the ACE-V30. However, "quadrant glitches" due to the friction still exist, which could be alleviated using feedforward compensation [6] in the future. The user-defined minimum bandwidth (12 Hz) was not violated even though the CLBW of each axis has been somewhat reduced as a result of the optimal search (Table 2). Thus, there was not a significant loss of tracking bandwidth.

6. Conclusions and discussion

Without using a complex motion controller that may not improve the performance meaningfully, an autotuning procedure of a P controller for feed-drive systems of a CNC vertical machining center was successfully implemented. Due to extremely large moving mass of traveling-column-type vertical machining center, the use of aggressive high-frequency perturbation signals was prohibited. The novel multiharmonic perturbation signal was smooth and informative enough; system identification of high-order discrete transfer functions was rapidly completed without upsetting the plant or violating travel limits. The discrete domain open-loop models are similar to those obtained using a random Gaussian sequence and step-sine sweep excitation. Power spectral estimate of the model transfer function was also close to one that was experimentally obtained. Formulation of prediction-error method was modified to ensure the stability of the open-loop poles owing to integrating action of a current controller in a servo drive. Also, the autotuning program shows the estimated poles and zeros to the end-user for examining model stability.

Using the numerical search method, the closed-loop bandwidth (CLBW) of each axis was maximized while keeping the model well damped. The CLBWs for the *x* and *z* axes are much improved compared to the results of the pole-placement method. A fine-tuning method based on an optimal search algorithm was also introduced. Unmatched closed-loop dynamics to a three dimensional circular trajectory were adjusted by fine-tuning the three feed axes simultaneously. As a result, contouring error was minimized. Using an optimal search method (i.e., steepest-descent algorithm), the optimal P gains were successfully and rapidly found. Using the automated fine tuning, the contour error is greatly reduced at all the tested feed rates (i.e., 0.5, 1, and 2 m/min), compared to the results of the other two design methods. Testing the fine-tuned P gains further with various trajectories (e.g., much faster circles, diamond, 3-D linear interpolation) is underway. Importantly, all the P-gain design steps yielded the closed-loop systems of which the predicted stability margins are satisfactory. All the tuning steps can be automated with minimal initial-parameter settings. The autotuning procedure could be implemented in similar motion control systems of machine tools, where the CLBW is typical (<25 Hz). Thus, the time and labor costs can be saved before commissioning, and the machine tools can be readily retuned by the end user.

The autotuning procedure presented here could be adapted for motion controller design for high-speed machining applications, where a higher tracking bandwidth is required (e.g., 100 Hz [4]). An advanced feedback controller (PD or PID) could be used to improve the CLBW. The extension of controller design including relevant feedforward controls (i.e., ZPTEC, friction compensation) for this purpose is also underway. Finally, more systematic and reliable approaches on the automated modeling (i.e., nonlinearity characterization on perturbation signal, automated comparison with the spectral estimate of input/output signal) will be also valuable in employing the multiharmonic signal for identification of a wider class of machine tools.

Acknowledgement

We would like to acknowledge Mr. Hansuk Kim for the help of frequency-domain system identification.

References

[1] Ulsoy AG, Koren Y. Control of machining processes. Journal of Dynamic Systems Measurement and Control 1993;115(2B):301–8.
[2] Erkorkmaz K, Altintas Y. High speed CNC system design. Part III: high speed tracking and contouring control of feed drives. International Journal of Machine Tools and Manufacture 2001;41(11):1637–58.
[3] Zirn O, Batzies E, Weikert S, Scholler T. State control of servo drives with flexible structural components. In: Proceedings of the 41st industry applications conference, vol. 4. Piscataway, NJ: IEEE; 2006. p. 1760–6.
[4] Hecker RL, Flores GM, Xie Q, Haran R. Servocontrol of machine-tools: a review. Latin American Applied Research 2008;38:85–94.
[5] Tomizuka M. Zero phase error tracking algorithm for digital control. Journal of Dynamic Systems, Measurement, and Control 1987;109(1):65–8.
[6] Lee HS, Tomizuka M. Robust motion controller design for high-accuracy positioning systems. IEEE Transactions on Industrial Electronics 1996;43(1):48–55.
[7] Endo S, Kobayashi H, Kempf CJ, Kobayashi S, Tomizuka M, Hori Y. Robust digital tracking controller design for high-speed positioning systems. Control Engineering Practice 1996;4(4):527–36.
[8] Erkorkmaz K, Altintas Y. High speed CNC system design. Part II: modeling and identification of feed drives. International Journal of Machine Tools and Manufacture 2001;41(10):1487–509.
[9] Astrom KJ, Hagglund T, Hang CC, Ho WK. Automatic tuning and adaptation for PID controllers – a survey. Control Engineering Practice 1993;1(4):699–714.
[10] Luo R, Qin SJ, Chen D. A new approach to closed-loop autotuning for proportional-integral-derivative controllers. Industrial and Engineering Chemistry Research 1998;37(6):2462–8.
[11] Hang CC, Sin KK. On-line auto tuning of PID controllers based on the cross-correlation technique. IEEE Transactions on Industrial Electronics 1991;38(6):428–37.
[12] Iwasaki T, Sato T, Morita A, Maruyama H. Auto-tuning of two-degree-of-freedom motor control for high-accuracy trajectory motion. Control Engineering Practice 1996;4(4):537–44.

[13] Inoue K, Nakaoka M. Autotuning gain parameter implementation with fuzzy learning control scheme for DC brushless servo system. IEE Proceedings – Control Theory and Applications 1998;145(5):419–27.
[14] Kobayashi S, Awaya I, Kuromaru H, Oshitani K. Dynamic model based auto-tuning digital servo driver. IEEE Transactions on Industrial Electronics 1995;42(5):462–6.
[15] Gyöngy IJ, Clarke DW. On the automatic tuning and adaptation of PID controllers. Control Engineering Practice 2006;14(2):149–63.
[16] Ziegler JG, Nichols NB. Optimum settings for automatic controllers. Transactions of the ASME 1942;64:759–68.
[17] Padhy PK, Majhi S. Improved automatic tuning of PID controller for stable processes. ISA Transactions 2009;48(4):423–7.
[18] Tung E, Tomizuka M. Feedforward tracking controller design based on the identification of low frequency dynamics. Journal of Dynamic Systems Measurement and Control 1993;115(3):348–56.
[19] Xiao S, Chen Y, Zheng G. Design and static performance of high speed machining centre with direct drive. Frontiers of Mechanical Engineering in China 2009;4(2):197–202.
[20] Fox PD, Godfrey KR. Multiharmonic perturbations for nonparametric autotuning. IEE Proceedings – Control Theory and Applications 2002;146(1):1–8.
[21] Poo AN, Bollinger JG, Younkin GW. Dynamic errors in type 1 contouring systems. IEEE Transactions on Industry Applications 1972;IA-8(4):477–84.
[22] Kim TY, Kim J. Adaptive cutting force control for a machining center by using indirect cutting force measurements. International Journal of Machine Tools and Manufacture 1996;36(8):925–37.
[23] Lee HS. Robust digital tracking controllers for high-speed/high-accuracy positioning systems. Ph.D. thesis, University of California at Berkeley; 1994.
[24] Altintas Y. Prediction of cutting forces and tool breakage in milling from feed drive current measurements. Journal of Engineering for Industry 1992;114(4):386–92.
[25] Weule H, Frank T. Advantages and characteristics of a dynamic feeds axis with ball screw drive and driven nut. CIRP Annals – Manufacturing Technology 1999;48(1):303–6.
[26] Tesfaye A, Tomizuka H. Zeros of discretized continuous systems expressed in the Euler operator – an asymptotic analysis. IEEE Transactions on Automatic Control 1995;40(4):743–7.
[27] Bamieh B. Intersample and finite wordlength effects in sampled-data problems. IEEE Transactions on Automatic Control 2003;48(4):639–43.
[28] Ljung L. System identification: theory for the user. Upper Saddle River, NJ, USA: Prentice Hall, Inc.; 1999.
[29] Schoukens J, Swevers J, Pintelon R, van der Auweraer H. Excitation design for FRF measurements in the presence of non-linear distortions. Mechanical Systems and Signal Processing 2004;18(4):727–38.
[30] Godfrey KR, Tan AH, Barker HA, Chong B. A survey of readily accessible perturbation signals for system identification in the frequency domain. Control Engineering Practice 2005;13(11):1391–402.
[31] Pritschow G. On the influence of the velocity gain factor on the path deviation. CIRP Annals – Manufacturing Technology 1996;45(1):367–71.
[32] Kuo BC. Automatic control systems. New York, NY, USA: John Wiley and Sons, Inc.; 2002.
[33] Choi B, Choi C, Lim H. Model-based disturbance attenuation for CNC machining centers in cutting process. IEEE/ASME Transactions on Mechatronics 1999;4(2):157–68.
[34] Arora JS. Introduction to optimum design. San Diego, CA, USA: Elsevier Academic Press; 2004.
[35] Havre K, Skogestad S. Effect of RHP zeros and poles on the sensitivity functions in multivariable systems. Journal of Process Control 1998;8(3):155–64.